

Enhancement of Entanglement Percolation in Quantum Networks via Lattice Transformations

G John Lapeyre, Jr.*

Jan Wehr

Department of Mathematics, The University of Arizona, Tucson, AZ 85721-0089, USA

Maciej Lewenstein

*ICFO-Institut de Ciències Fotòniques, Mediterranean Technology Park, E-08860 Castelldefels (Barcelona), Spain
ICREA-Institució Catalana de Recerca i Estudis Avançats, Lluís Companys 23, 08010 Barcelona, Spain*

(Dated: July 14, 2008)

We study strategies for establishing long-distance entanglement in quantum networks. Specifically, we consider networks consisting of regular lattices of nodes, in which the nearest neighbors share a pure, but non-maximally entangled pair of qubits. We look for strategies that use local operations and classical communication. We compare the classical entanglement percolation protocol, in which every network connection is converted with a certain probability to a singlet, with protocols in which classical entanglement percolation is preceded by measurements designed to transform the lattice structure in a way that enhances entanglement percolation. We analyze five examples of such comparisons between protocols and point out certain rules and regularities in their performance as a function of degree of entanglement and choice of operations.

PACS numbers: 03.67.-a, 03.67.Bg, 64.60.ah

I. INTRODUCTION

Entanglement is the property of states of multipartite quantum systems that is the most important resource for quantum information processing [1]. For this reason, one of the most important tasks of quantum information science is to establish entanglement at long distances in quantum networks, and to optimize final entanglement and probability of success.

Quantum networks [2, 3] play a key role in quantum information processing. Here we limit our attention to those networks in which quantum states can be prepared initially and shared. That is, entanglement can be generated between neighboring or, at least, not-too-widely-separated nodes (or stations). There are two instances in which the above-mentioned tasks become obviously relevant. On one hand, one can consider macroscopic quantum communication networks, such as cryptographic networks, or more generally quantum communication nets [4, 5, 6], or distributed quantum computation [7] involving arbitrary nodes of the network. The second instance concerns microscopic or mesoscopic networks that could constitute architectures of quantum computers (cf. Ref. 8).

Despite enormous progress in experimental techniques (cf. Ref. 6 and references therein), it is in principle a very hard task to establish entanglement at large distances due to decoherence and attenuation effects. Two remedies for this problem have been proposed:

- *Quantum repeaters.* This concept has been developed for 1D quantum communication chains [9, 10, 11, 12]. Although the simple entanglement swapping [13] procedure can lead to quantum communication at large distances (see Fig. 1), for imperfect resources, the performance of such communication chains decays exponentially with the distance (i.e. the number of repeaters). However, one can use more sophisticated quantum repeater protocols, which use purification and swapping methods that lead to polynomial decay only.
- *Entanglement percolation.* Recently, our collaborators, together with two of us, proposed using networks in which properties of the connectivity of the network enable the establishment of, and determine the probability of, entanglement on large distances. In Refs. 14 and 15 we considered in particular *pure-state networks* on regular lattices, where the nearest-neighbor (NN) nodes share a non-maximally entangled pair of qubits, or more generally qudits (an entangled bond). We searched for local operations and classical communication (LOCC) protocols that lead to establishment of entanglement between remote nodes of the network.

At present, only a handful of studies that explicitly apply percolation theory to problems in quantum information have appeared in the literature. These articles, comprising Refs. 14 and 15 as well as applications to cluster states, are reviewed in Ref. 16.

Our results leading to the present work can be summarized as follows:

- For 1D chains we proved that even optimal LOCC

*Electronic address: lapeyre@physics.arizona.edu

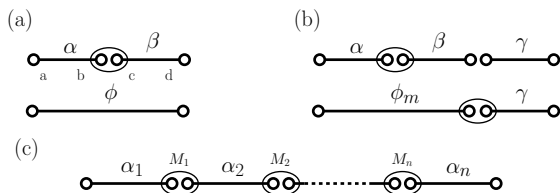


FIG. 1: Entanglement swapping and 1D repeater. Circles are qubits. Heavy lines represent pure non-maximally-entangled states. Loops represent the entanglement swapping measurement on a pair of qubits. a) Two states α and β of the form specified in (1). After the operation, qubits a and d may be in an entangled, mixed state. b) swapping as the first step in a repeater. c) a 1D chain of repeaters.

strategies only allow the establishment of entanglement between distant nodes that decays exponentially with both the distance, as well as the quality of entanglement of NN bonds.

- In 2D and higher dimensions, the possibilities for protocols are greatly expanded. The most straightforward, naive protocol—the one we use as a baseline to evaluate other protocols—is the one we term *classical entanglement percolation* (CEP), although it does involve obviously some quantum operations. This protocol begins with converting (using LOCC) each of the entangled bonds into a singlet (*i.e.* maximally entangled state) with probability p (the so-called singlet conversion probability (SCP) [17, 18]). Each of the parties (nodes) knows obviously which of the bonds are now perfectly entangled. Using classical communications, the parties establish whether there exists an infinite (large size) percolating cluster and who belongs to it. Then, by performing a series of entanglement swappings, it is possible to propagate entanglement between any two (widely) separated nodes that belong to the percolating cluster. We call this scheme “classical” because it essentially maps the problem onto a classical bond percolation problem [19], and its success or failure is equivalent to the success or failure of the bond percolation in the same lattice. Namely, if $p > p_c$, where p_c is the lattice-dependent critical percolation threshold (or, in other words, critical open-bond density), then entanglement between any two remote nodes can be established with probability $P > 0$, which asymptotically does not depend on the distance.
- At the same time that we introduced CEP, we presented several schemes that went beyond the simple application of singlet conversion everywhere followed by entanglement swapping along a path. We call these *quantum entanglement percolation* (QEP) protocols because they use some kind of quantum pre-processing—for instance quantum measurements to transform one percolation problem to

another one. In these protocols CEP is also used, but is preceded by application of certain LOCC, which remove and replace bonds in the network lattice, resulting in a new lattice geometry with fundamentally different long-range properties. The pre-processing in QEP may greatly improve the possibility of entanglement percolation, either by reducing p_c , or by increasing P .

In this paper we present a more systematic and thorough study of QEPs based on lattice transformations. In particular, we explore the entire parameter space with the addition of Monte Carlo and series-expansion methods. Although we do not find a general principle, we do discover certain rules and regularities governing such strategies (see Sec. III). The paper is organized as follows. In Sec. II we formulate and describe the models and fix the notation. Section II A discusses quantum networks and percolation, whereas Sec. II B deals with LOCCs used for lattice transformations. Our main results are presented in Sec. III, which contains descriptions of five examples of transformations enhancing CEP: i) the transformation of the kagomé lattice to the square lattice, ii) the transformation of the double-bond honeycomb (hexagonal) lattice to the triangular lattice, iii) the transformation of the square lattice to two decoupled copies of the square lattice, iv) the transformation of the bowtie lattice to the decoupled triangular and square lattices, and v) the transformation of a triangular lattice with two different degrees of entanglement into the decoupled square and triangular lattices. The cases ii), iii), and v) were discussed already in Ref. 15, but we present here more general and stronger results. We conclude in Sec. IV.

Over the past few decades, classical percolation theory has seen the development of a number of quite sophisticated and powerful methods, which we have adapted to the questions at hand. In order to demonstrate the supremacy of QEP over CEP in each of the cases i)-v) we employ these methods combined with the methods of quantum information theory. An overview of these methods is presented in the appendices: Appendix A presents the necessary facts from majorization theory and singlet conversion protocols [18], Appendix B explains some details of our Monte Carlo (MC) simulations, and finally Appendix C deals with series expansions.

II. FORMULATION OF THE MODELS

A. Quantum networks and percolation

In this section, we describe the classes of quantum networks and communication protocols that we investigated.

1. Networks of bipartite states

The networks we consider consist, prior to application of communication protocols, of a collection of qubits partitioned into pairs, each pair being prepared in an identical pure state $|\alpha\rangle \in \mathbb{C}^2 \otimes \mathbb{C}^2$. With appropriate choice of bases, any such state can be written

$$|\alpha\rangle = \sqrt{\alpha_0}|00\rangle + \sqrt{\alpha_1}|11\rangle, \quad (1)$$

where the Schmidt coefficients α_0, α_1 satisfy $\alpha_0 \geq \alpha_1$ and $\alpha_0 + \alpha_1 = 1$. These pairs can be identified with bonds on a two-dimensional lattice or edges on a graph, with two spatially-separated qubits, one occupying each end of the bond. At regular positions, a small set of these qubits are arranged near enough to one another to allow measurements on any subset. Such a set of qubits then constitutes a vertex (or node or site) which is incident to each edge that contributes a qubit to the vertex. This defines a lattice to which we apply methods of statistical physics. In particular, many results on the possibility of long-range entanglement are described using percolation theory [19, 20], and depend only on the graph structure of the system.

2. Classical entanglement percolation

Given a lattice prepared as described above, we search for the protocols consisting of local operations and classical communication (LOCC) that yield the maximum probability of achieving entanglement between two nodes separated by an arbitrarily large distance. The answer depends on the single parameter α_1 characterizing the state $|\alpha\rangle$. Even with a small palette of possible operations, finding the globally optimal solution is a difficult task. Instead, we search for promising classes of protocols. The simplest protocol consists of attempting to convert the state associated with each bond to a singlet via the ‘‘Procrustean method’’ of entanglement concentration, which is the optimal strategy [17, 18]. This conversion succeeds with probability $p = 2\alpha_1$ (See Appendix A.), while failure leaves the pair in a state with no entanglement. In this way the system is described exactly by a bond percolation process with open-bond density p . If there is a path of open (maximally entangled) bonds connecting two nodes, a sequence of entanglement swapping measurements, one at each intermediate node, is then applied in order to entangle the first and last node. This protocol is the simplest example of classical entanglement percolation.

3. Percolation theory for CEP.

Here we review a few fundamental ideas in percolation theory necessary to analyze CEP. The nodes in the lattice can be partitioned into sets such that each node within a

set is connected to each other node in the set via a path of open bonds. Such a set of nodes is called an open cluster, or sometimes simply a cluster. The central fact of percolation theory is that percolation processes on most commonly studied lattices in dimension 2 and higher exhibit a continuous phase transition as the bond density passes through a critical value p_c . For $p > p_c$ there exists with probability one a unique (for the lattices we study here) cluster of infinite mass (number of nodes), while for $p < p_c$ all clusters are finite with probability one. It follows that improving an LOCC protocol to obtain a small change in p can have a dramatic effect on the probability of long-range entanglement. In the supercritical phase, long-range entanglement is possible, while in the subcritical phase it is not possible. Serving as the order parameter is the density of the infinite cluster $\theta(p)$ which we define via

$$\theta(p) = P[A \in \mathcal{C}], \quad (2)$$

the probability that a fixed node A (say, the origin) is in the infinite cluster \mathcal{C} . When referring to θ on a specific lattice, we use a symbol representing the lattice as a subscript. The probability that two selected nodes are members of the same cluster decays roughly exponentially in their separation distance with a length scale $\xi(p)$ (the correlation length) to $\theta^2(p)$. This means, for the problem at hand, that in CEP the probability that information can be propagated between two nodes is asymptotically $\theta^2(p)$.

B. Transformations of lattice structure

It was proven in Refs. 14 and 15 that CEP is not the optimal strategy for establishing long-distance entanglement. The demonstration is based on applying certain LOCC prior to CEP. All of these pre-processing LOCC act on pairs of qubits, i.e. involve bipartite systems, and they either transform the state on a given bond, or they replace two adjacent pure-state bonds by one, in general, mixed state bond.

There are essentially three types of generalized measurement used:

- *Singlet conversion* The optimal LOCC singlet protocol [18] is used in three situations. In CEP with single-bond lattices we apply it directly to the state (1), which results in the singlet conversion probability $p = 2\alpha_1$. If the protocol is successful, the bond that is converted to the singlet can be used for entanglement propagation (swapping), otherwise it is useless. In CEP with a double-bond lattice we apply it directly to the two copies of the state (1), which lives in $\mathcal{C}^4 \otimes \mathcal{C}^4$, and has Schmidt coefficients $\alpha_0, \sqrt{\alpha_0\alpha_1}, \sqrt{\alpha_0\alpha_1}, \alpha_1$, ergo the singlet conversion probability is

$$p = \min \{1, 2(1 - \alpha_0^2)\}. \quad (3)$$

Finally, in all of the QEP strategies that we study, we also apply singlet conversion to any remaining untouched bonds after the lattice transformation.

- *Entanglement swapping* This protocol [13], illustrated in Fig. 1a, consists of performing the so-called Bell measurement on a pair of qubits (b and c) in a node, i.e. von Neumann measurement in a basis of 4 maximally entangled orthonormal states (in the computational basis). It allows conversion of a pair of adjacent singlets into a singlet connecting end points (a and d) with probability 1, i.e. allows for perfect entanglement propagation in a connected cluster of singlets. At the same time, when applied to a pair of imperfect states (1), it produces a mixed state, which, amazingly, has the average singlet conversion probability equal to $p = 2\alpha_1$. Unfortunately, this effect cannot be iterated. When applied to the mixed states, entanglement swapping reduces the singlet conversion probability. This last point places a significant constraint on our choice of lattice transformations.

We use entanglement swapping in both CEP and QEP, but the two uses have very different effects. In the case of CEP, entanglement swapping is used to locally move entanglement between neighboring nodes, an operation that is repeated in hopes of transporting entanglement over long distances (This is, roughly speaking, a brute-force method). But with QEP, before attempting to transfer entanglement, we search for a way to selectively apply entanglement swappings to alter the geometry of the lattice and hence its long-range connectivity properties as given by percolation theory. The goal of this paper and future work is to enumerate the rich possibilities and point a way towards a general description of QEP.

- *Worst case entanglement* Finally, in Refs. 14 and 15 the worst case protocol was used, which maximizes minimal entanglement over all measurement outcomes. This protocol consists also of Bell measurement, but the basis is computational for one qubit, and corresponding to eigenstates of σ_x for the second. When applied to qubits, it produces a mixed state with the property that for all measurement outcomes, the resulting pure states have the same singlet conversion probability. We will not use this protocol here.

In order to describe the lattice transformations involved in QEP, we need a more general formulation of the lattice than the one given in Sec. IIA 1 for CEP. It is useful to define the percolation processes a bit more precisely. We begin with a graph, that is, a set of edges (bonds) E and a set of vertices (nodes) V . We consider embedding the graph in \mathbb{R}^2 in order to treat geometric properties. In fact, the important properties don't change if we force the vertices to occupy points in \mathbb{Z}^2 .

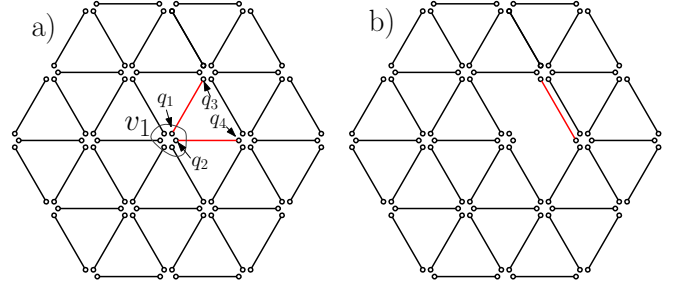


FIG. 2: a) Mapping a quantum network to a percolation problem. Qubits are represented by small circles. Each vertex (node) contains six qubits. b) using entanglement swapping to transform the lattice structure. The two gray (red in color) bonds in a) are replaced by the red bond in b). This process can be continued to produce a double-bond hexagonal lattice.

The configuration of open and closed bonds can be described by a probability sample space $\Omega = \prod_{e \in E} \{0, 1\}$, with points $\omega = (\omega(e) : e \in E)$, where $\omega(e)$ takes the values 0 and 1. We allow each bond to be open with a different probability, i.e. $\mathbf{p} = (p(e) : e \in E)$. The appropriate measure is a product measure on Ω with marginal probabilities defined by $\mu_e(\omega(e) = 1) = p(e)$, $\mu_e(\omega(e) = 0) = 1 - p(e)$. To allow all transformations possible via LOCC, we take the graph to be complete—that is, all possible edges $e = \langle v, w \rangle$ with $v, w \in V$ are present (In fact, sometimes we need double bonds, as well.) For percolation properties, any graph with fewer edges can be identified with this complete graph by setting the appropriate $p(e)$ to zero.

Now we describe the correspondence of entanglement on the physical system of qubits to this percolation formulation. We denote the set of the indices of all qubits by A . Each qubit $a \in A$ is assigned to a vertex $v = V(a)$, with, in general, multiple qubits assigned to each vertex. For example, a portion of a network that can be described by a triangular lattice is shown in figure Fig. 2a, where vertex v_1 contains the six circled qubits. For every pair of qubits $a, b \in A$ with $V(a) \neq V(b)$, we denote the reduced state by ρ_{ab} , and by $S(a, b)$ the singlet conversion probability (SCP), that is, the probability of conversion of ρ_{ab} to a singlet, maximized over all possible measurements. Then we assign $p(e) = S(a, b)$ for every $e = \langle V(a), V(b) \rangle$. Initially, all reduced bipartite states have either $p(e) = 0$ for separable states, or $p(e) = p = 2\alpha_1$ for the prepared, pure, partially entangled states. In Fig. 2a the edges with $p(e) = p$ are shown in black, while edges with $p(e) = 0$ are simply absent in the diagram. Two bonds are colored gray (red in color) only to show that they will be replaced by another bond (in the sense of altering the SCP) via entanglement swapping. For QEP, a successful preprocessing, entanglement swapping operation such as that depicted in Fig. 1, alters the percolation process by setting $p(\langle V(a), V(b) \rangle) = 0$ and $p(\langle V(c), V(d) \rangle) = 0$ and $p(\langle V(a), V(d) \rangle) = p$. Likewise, in the example in Fig. 2, an entanglement swapping measurement on qubits q_1 and

q_2 sets $p(\langle V(q_1), V(q_3) \rangle) = 0$, $p(\langle V(q_2), V(q_4) \rangle) = 0$, and $p(\langle V(q_3), V(q_4) \rangle) = p$. Each of the examples discussed below conforms to this description.

III. EXAMPLES

We consider five examples of lattice transformations in this paper, each exhibiting a different combination of features, with implications for the analysis of protocols. In particular, two transformations convert one lattice to another, while the other three convert a lattice into two decoupled lattices. Four transformations involve lattices with single bonds, while the fifth involves double bonds. Quantities arising in the analysis, such as $\theta(p)$, are analytic about $p = 1$. In fact, the lowest-order term in the expansion about $p = 1$ is typically much larger than the remaining terms even relatively far from $p = 1$, with the result that most of the interesting crossover behavior in comparing protocols occurs for smaller values of p . But this behavior does not appear when using the distillation procedure for double bonds that leads to (3). The reason is that distillation produces a saturation point for $\theta(p)$ smaller than $p = 1$. This results in a much stronger difference between classical and quantum protocols in the high-density regime than does singlet conversion on single bonds (two-qubit pure states). Four of the transformations produce a smaller critical density on at least one of the resulting lattices, which gives the most pronounced advantage in the regime near the critical density. The fifth example shows that on some lattices where a particular QEP strategy is not advantageous, allowing bonds of different strengths p and p' can produce regions in the phase space (p, p') where QEP is indeed advantageous. Finally, consider comparing CEP in which singlet conversion is applied to each bond separately, with QEP that results in a single transformed lattice. In every such case we find that QEP is better than CEP over the entire (non-trivial) range of p . It is an open question whether this is generic behavior.

We analyze the results of the transformation of each lattice in three regimes: near the critical density (or densities); near $p = 1$; and between these two regimes. Arguments near the critical densities typically rely simply on the fact that long-range entanglement is impossible on a lattice with density below the critical density. These results are the most insensitive to details of the definitions of entanglement and connectivity. Near $p = 1$ we compute high-density expansions for $\theta(p)$ and related quantities (see Sec. C.) Often the difference between the performance of CEP and QEP in this regime is marginal. It is important nonetheless to carry out the analysis if we hope to make general statements about transformations that hold for all p . Between the critical regime and high-density regime there are some techniques widely used in percolation theory that may be useful, such as Russo's formula, which is used to prove inequalities in the rate of change of $\theta(p)$. However, we leave these techniques for

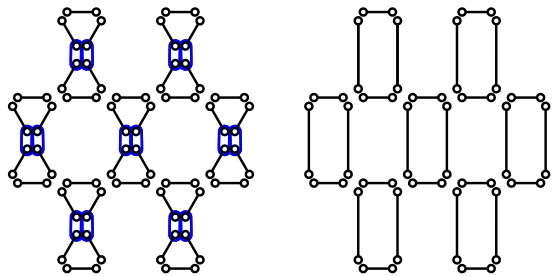


FIG. 3: One of three transformations of the kagomé lattice to the square lattice. Pairs of qubits that are subjected to entanglement swapping are marked with loops.

future work and use Monte Carlo computations in the present paper.

A. Kagomé lattice to square lattice

In our first example we compare CEP on the kagomé lattice to quantum entanglement percolation consisting of transformation of the kagomé lattice to the square lattice via entanglement swapping at nodes specified in Fig. 3. Although we do not treat them here, there are at least two more ways to transform the kagomé lattice to the square lattice using the same kind of entanglement swapping. Rigorous bounds have been obtained for $p_c(\text{kagomé})$ [19] (As well as a high-precision Monte Carlo estimate [21].) while $p_c(\square)$ is known exactly, proving that the transformation gives an advantage for p lying between $p_c(\square)$ and the lower bound for $p_c(\text{kagomé})$. As shown in Table II, the series for θ_\square and θ_{kag} are the same to the first non-trivial order in $q = 1 - p$. But the next term shows that $\theta_\square > \theta_{\text{kag}}$ for p close enough to 1. The MC data provides strong evidence that $\theta_\square > \theta_{\text{kag}}$ everywhere except near $p = 1$, where the statistical error is too large to distinguish the curves. But as is evident from the lower plot in Fig. 3, the terms in the expansions that we computed dominate $\theta_\square - \theta_{\text{kag}}$ already at values of p for which the MC data is still accurate. Thus we find that QEP is advantageous over the entire range of p .

B. Double-bond hexagonal lattice to triangular lattice

The hexagonal lattice with double bonds, each in the state specified by (1) (see Fig. 5a), was discussed in Refs. 14 and 15, in which it was shown that a transformation of the lattice to a triangular lattice offers an advantage over CEP protocols for values of p between $p_c(\triangle)$ and another critical value defined below. Here we extend the analysis to determine over the entire range of p which of three protocols gives the highest probability of long-range entanglement. The first of the three protocols, which we call CEP I, consists of performing an optimum

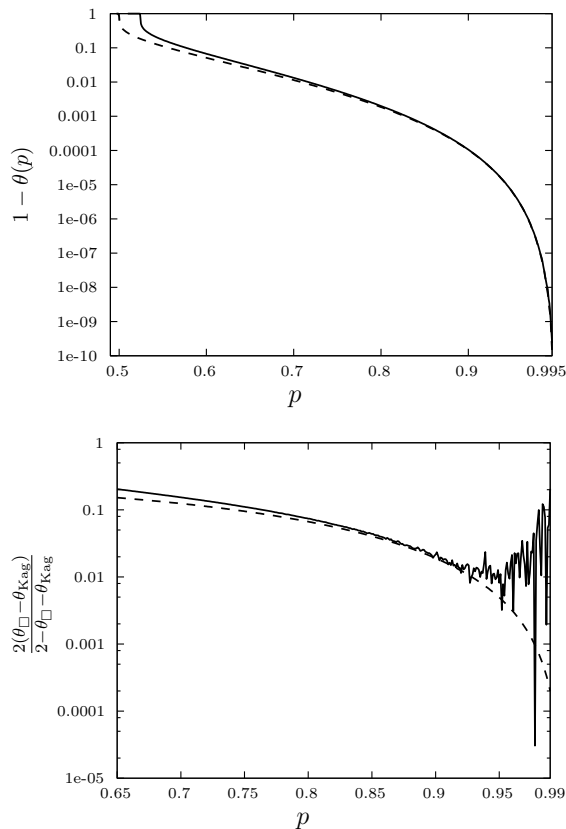


FIG. 4: Upper plot: Monte Carlo of $1 - \theta(p)$ v.s. $p = 2\alpha_1$. The solid line is on the square lattice. The dashed line is on the kagomé lattice. Lower plot: Normalized difference between θ_{\square} and θ_{kag} . The solid line is computed from MC data. The dashed line is computed from expansions from Table II.

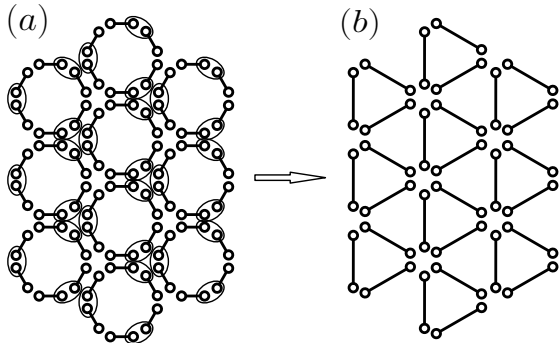


FIG. 5: (a) Double-bond hexagonal lattice. (b) transformed into the triangular lattice (b). Pairs of qubits that are subjected to entanglement swapping are marked with loops.

singlet conversion to each bond separately so that the probability of getting at least one singlet connecting two nodes is $p' = 1 - (1 - p)^2$. Communication on the resulting lattice is then determined by bond percolation on the hexagonal lattice with bond density p' . In particular, the critical density (see Table I) is $p = p_c(\text{CEP I}) \approx 0.4107$. In the second protocol, we perform a more efficient conversion, namely distillation, on all four qubits in a double

bond. This protocol succeeds in producing a maximally entangled pair with probability $p'' = \min\{1, 2(1 - \alpha_0^2)\}$ (See (3) and Appendix A.) This results in bond percolation on the hexagonal lattice with density

$$p'' = \min \left\{ 1, 2 \left[1 - \left(1 - \frac{p}{2} \right)^2 \right] \right\}. \quad (4)$$

We refer to this method as CEP II, with critical density $p = p_c(\text{CEP II}) \approx 0.358$. In the third method, the entanglement swapping that maximizes SCP is applied at every other node (see Fig. 5), converting the double-bond hexagonal lattice to the triangular lattice with bond density p , with $p_c(\triangle) \approx 0.347$.

The three protocols are compared in Fig. 6. We first observe that each method fails below its corresponding critical density, and these are known exactly. To compare the methods away from the critical points, we computed series expansions of $\theta(p)$ about $q = 0$ with results listed in Table II. Defining $\tilde{\theta}(q) = \theta(1 - q)$ we see that

$$\tilde{\theta}_{\text{CEP I}}(q) = \tilde{\theta}_{\square}(q^2) = 1 - q^6 - 3q^8 + \dots \quad (5)$$

Comparing (5) to $\theta_{\triangle}(p)$ from Table II we see that for $p \rightarrow 1$ the conversion to the triangular lattice is better than CEP I. As is evident from Figs. 6a and 6b, the two curves have the same leading behavior as $p \rightarrow 1$, with the result that the Monte Carlo cannot distinguish them in this region. However, the series expansion lies well within the statistical error of the Monte Carlo points, even relatively far from $p = 1$, so we can be confident that $\theta_{\triangle} > \theta_{\text{CEP I}}$ even in the region where the MC cannot distinguish the curves. Finally, the MC clearly shows that $\theta_{\triangle} > \theta_{\text{CEP I}}$ for smaller p , where the expansion fails. Turning now to CEP II, we know that $\theta_{\triangle} > \theta_{\text{CEP II}}$ for $p_c(\triangle) < p < p_c(\text{CEP II})$ and from (4) that $\theta_{\text{CEP II}} = 1$ for $p \geq 2 - \sqrt{2}$. It follows that there must be a crossover point. The MC data suggests that this occurs for $p \approx 0.375$. In summary, we see that QEP gives an advantage over CEP I for all p , but that CEP II, which is more efficient in its use of double bonds, is better than QEP at high densities.

C. Square lattice to two decoupled copies of the square lattice

This transformation replaces the square lattice with two decoupled copies of the square lattice. To effect the transformation, at selected nodes the two horizontally opposing bonds are joined into one bond and likewise with the vertically opposing bonds. This procedure is applied at every other node, while staggering by one node when shifting rows as shown in Fig. 7. Because the transformation splits the original lattice into two disjoint lattices, each taking half the surviving nodes, we cannot compare connection between a single pair of nodes before and after the transformation. Rather, we consider on the original lattice connection between, on the one hand, a

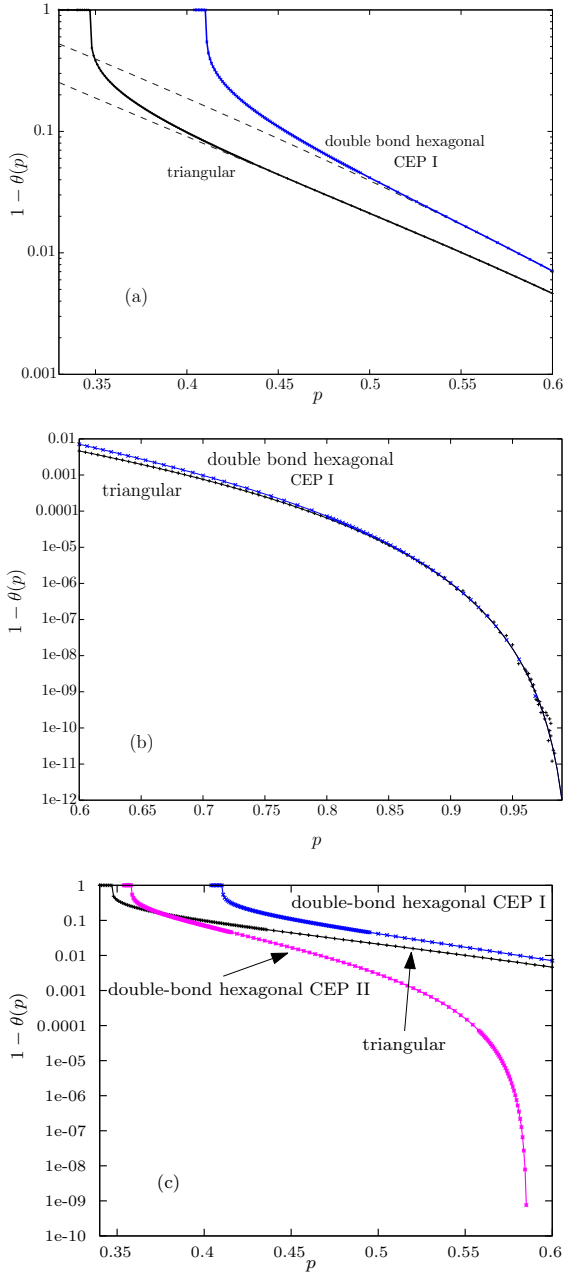


FIG. 6: Monte Carlo and series expansions about $p = 1$ of $1 - \theta(p)$ v.s. $p = 2\alpha_1$ for various strategies on the double-bond hexagonal lattice. (a) Solid lines are Monte Carlo data. Dashed lines are series expansions. (b) Solid lines are MC. Series expansions are indistinguishable from MC over the entire plot. (c) Monte Carlo data.

pair of nodes A, A' separated by a small distance, and on the other, the same pair translated a distance much larger than the correlation length to a pair B, B' . We choose A and A' so that each one goes to a different lattice in the transformation. After the transformation, there is the possibility of connection between A and B on one lattice and between A' and B' on the other. We choose the nodes as shown in Fig. 7. In addition to the

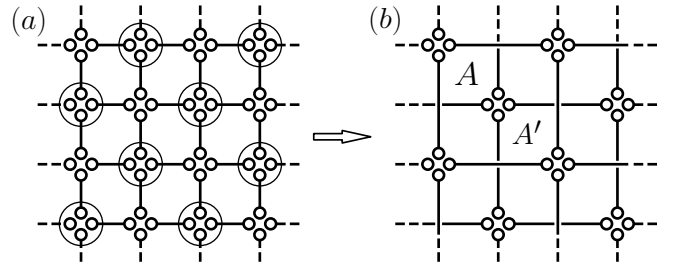


FIG. 7: Doubling the square lattice. Large circles represent nodes at which entanglement swapping is performed.

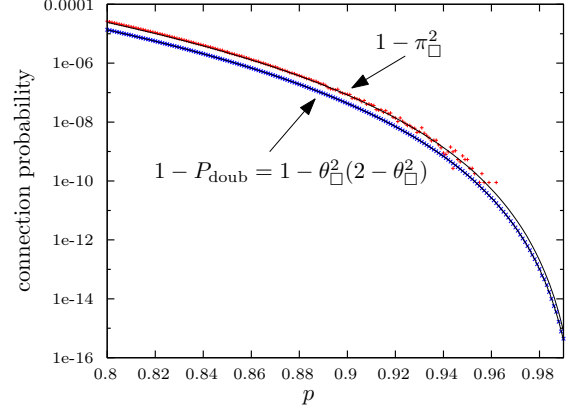


FIG. 8: Monte Carlo and series expansions for doubling the square lattice. Lower points: $1 - P_{\text{doub}}$ v.s. p . Upper points: $1 - \pi_{\square}^2$ v.s. p . Solid lines are series expansions.

complication of splitting, this example is subtle because the critical density is the same on all three lattices. In Ref. 15 it was shown that just above $p_c(\square) = 1/2$, the transformation gives an advantage over CEP as measured by the choice of nodes A, A' .

Here we examine the connectivity for all $p > p_c(\square)$. The probability that at least one of the pairs on the de-

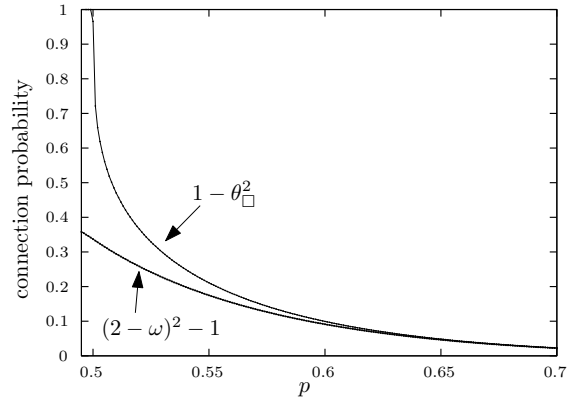


FIG. 9: Monte Carlo for doubling the square lattice. Upper points: $1 - \theta_{\square}^2$ v.s. p . Lower points: $(2 - \omega)^2 - 1$ v.s. p .

coupled lattices is connected is

$$P_{\text{double}} = 1 - (1 - \theta_{\square}^2)^2 = \theta_{\square}^2(2 - \theta_{\square}^2).$$

We compare P_{double} to the probability on the original lattice that at least one of A and A' is connected to at least one of B and B' . This probability is π_{\square}^2 where

$$\pi_{\square} = P[A \in \mathcal{C} \text{ or } A' \in \mathcal{C}]. \quad (6)$$

(In this paper ‘or’ in ‘ X or Y ’ does *not* mean exclusive or.) We prove that the doubling is advantageous in the limit $p \rightarrow 1$ using the power series about $q = 0$ for θ_{\square} and π_{\square} given in Table II. This follows from observing

$$\pi_{\square}^2 = 1 - 8q^8 - 36q^{10} + \dots$$

and

$$\theta_{\square}^2(2 - \theta_{\square}^2) = 1 - 4q^8 - 32q^{10} + \dots$$

Moreover, Monte Carlo evidence suggests that the transformation improves on CEP for all $p > p_c(\square)$. In Fig. 8 one sees from the accuracy of the series expansion in the region of high-quality MC data that the advantage is maintained even when the Monte Carlo becomes noisy near $p = 1$. The same MC data is not useful near $p_c(\square)$ for two reasons. Firstly, both P_{doub} and π_{\square}^2 vanish at the same critical point with infinite slope. Secondly, the systematic error due to finite lattice size and large fluctuations in cluster statistics further complicate distinguishing the curves. We instead make use of an alternate expression for π , that is $\pi_{\square} = \theta_{\square}(2 - \omega)$ where $\omega = P[A \in \mathcal{C} | A' \in \mathcal{C}]$. The condition for advantage over CEP then becomes

$$(2 - \omega)^2 < 2 - \theta_{\square}^2. \quad (7)$$

The MC data for ω was generated by considering the largest cluster in the finite lattice to represent the infinite cluster \mathcal{C} even if it is not a spanning cluster. The MC data supports (7), and furthermore, shows no evidence of non-analyticity at $p_c(\square)$, as is evident in Fig. 9.

The foregoing analysis of the doubled square lattice was based on the choice of A, A' shown in Fig. 7. But this is not the only reasonable choice. In fact the question of whether the doubling transformation is better than CEP depends somewhat on the details of how the nodes are chosen. Although this is an extreme example, similar questions arise in analyzing other transformations. Thus, the ambiguity in the measures comparing the various protocols must be addressed in future work.

D. Bowtie lattice to decoupled triangular and square lattices

This is our second example that transforms a lattice into two decoupled lattices. Figure 10 shows the measurements that decouple the bowtie lattice into the

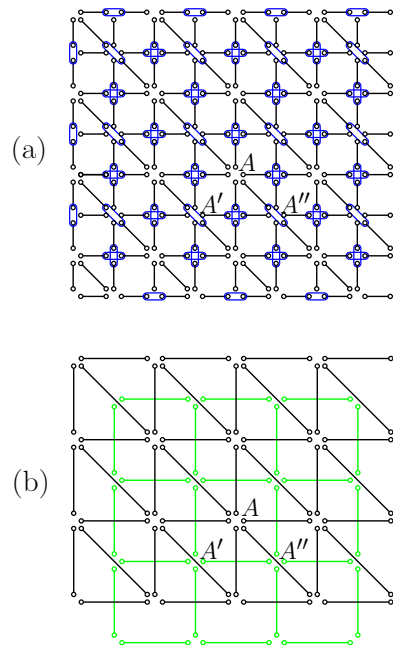


FIG. 10: Transformation of the bowtie lattice to decoupled square and triangular lattices. Loops marking pairs of qubits represent swapping measurements.

square lattice and the triangular lattice. For p satisfying $p_c(\triangle) < p < p_c(\bowtie)$ (the exact critical values are listed in Table I), the transformation is obviously advantageous.

In carrying out further analysis, the bowtie lattice presents a complication not present in other lattices studied in this paper: While the other lattices are regular in the sense that each vertex has the same environment up to rotations and reflections, the bowtie lattice has two kinds of vertices in this sense. Notice first that all the surviving nodes on the square and triangular lattices shown in Fig. 10 were generated from nodes of coordination number $z = 6$ on the bowtie lattice, with all nodes of $z = 4$ disappearing. Each node of $z = 6$ on the bowtie lattice has four nearest neighbors of $z = 6$, discounting nodes of $z = 4$ (for example node A in Fig. 10.) Furthermore, two of these nearest neighbors are connected by a diagonal bond (node A'') and two are not (node A').

In treating the example of doubling the square lattice in Sec. III C, the fact that the lattice decouples forced us to consider connections between two widely separated pairs of nodes. We treat the present example in the same way, except that the more complicated local structure of the bowtie lattice forces us to consider a cluster of three nodes A, A', A'' rather than a pair. In Fig. 10b we see that A', A'' are sent to the square lattice and A is sent to the triangular lattice. We consider a distant cluster of nodes B, B', B'' related to A, A', A'' by translation, and examine the probability that a connection exists between at least one of A, A', A'' and at least one of B, B', B'' . On the bowtie lattice, this probability is π_{\bowtie}^2 where

$$\pi_{\bowtie} = P_{\bowtie}[A \in \mathcal{C} \text{ or } A' \in \mathcal{C} \text{ or } A'' \in \mathcal{C}]. \quad (8)$$

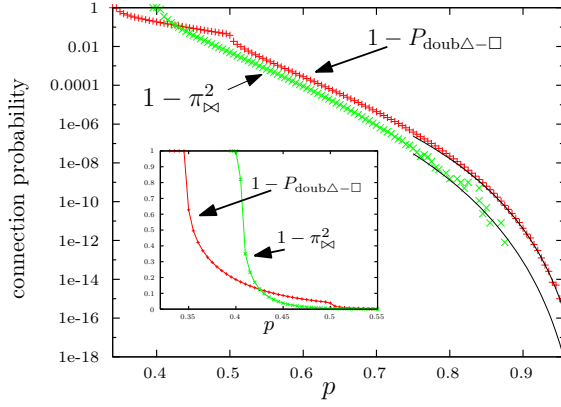


FIG. 11: Monte Carlo estimates of π_{\boxtimes} and $P_{\text{doub}\Delta-\square}$. The inset is the same data on a linear scale. Solid lines are high-density expansions.

Lattice	p_c for bond percolation
triangular	$2 \sin(\pi/18) \approx 0.347$
bowtie	≈ 0.4045
square	0.5
kagomé	≈ 0.5244053 MC estimate
hexagonal	$1 - 2 \sin(\pi/18) \approx 0.653$

TABLE I: p_c for bond percolation on some lattices. $p_c(\boxtimes)$ is the unique root of $1 - p - 6p^2 + 6p^3 - p^5$. All critical densities are exact[19] except for $p_c(\text{kagomé})$ [21].

If instead we decouple the lattices via the lattice transformation, this probability is given by

$$P_{\text{doub}\Delta-\square} = \theta_{\Delta}^2 + \pi_{\square b}^2 - \theta_{\Delta}^2 \pi_{\square b}^2,$$

where

$$\pi_{\square b} = P_{\square}[A' \in \mathcal{C} \text{ or } A'' \in \mathcal{C}]. \quad (9)$$

A comparison of Monte Carlo estimates and high-density expansions of these quantities is shown in Fig. 11. The MC data shows that for small densities, the lattice transformation gives an advantage, while for higher densities CEP is the better protocol. The cross-over occurs at $p \approx 0.425$. As with the other examples, the curves representing the series expansions suggests that no cross-over occurs in the high-density region.

E. Asymmetric triangular lattice

With this example we demonstrate that QEP can succeed when the initial bonds are not all in the same state, but fail if they are in the same state. Consider the lattice in Fig. 12a composed of two different kinds of bonds, each of the form given by (1). The solid and dashed bonds represent the states $|\alpha\rangle$ (with $p = 2\alpha_1$) and $|\alpha'\rangle$ (with $p' = 2\alpha'_1$) respectively. In general, $p \neq p'$.

$\theta_{\square}(p)$	$1 - q^4 - 4q^6$
$\pi_{\square}(p)$	$1 - 4q^8 - 18q^{10}$
$\pi_{\square b}(p)$	$1 - q^6 + q^7 - 8q^8$
$\theta_{\Delta}(p)$	$1 - q^6 - 6q^{10} + 6q^{11} - 6q^{12} - 21q^{14} + 42q^{15}$
$\theta_{\square}(p)$	$1 - q^3 - 3q^4 - 6q^5 - 25q^6$
$\theta_{\text{kag}}(p)$	$1 - q^4 - 6q^6$
$\pi_{\boxtimes}(p)$	$1 - 4q^{14}$

TABLE II: A few terms in series expansions about $q = 0$ of π and θ for various lattices. $\theta_{\square}, \theta_{\Delta}, \theta_{\square}, \theta_{\text{kag}}$ are defined via (2). $\pi_{\square b}$ is defined via (9), π_{\square} via (6), and π_{\boxtimes} via (8).

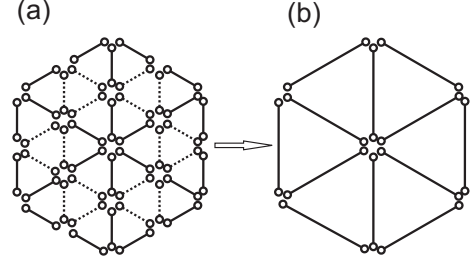


FIG. 12: a) The asymmetric triangular lattice. Solid bonds represent the state $|\alpha\rangle$ (density p). Dashed bonds represent the state $|\alpha'\rangle$ (density p'). b) Entanglement swapping is performed on pairs of solid bonds resulting in a triangular lattice with bond density p . The remaining dashed bonds form a kagomé lattice which is then transformed into a square lattice with bond density p' as in Sec. III A.

We consider two entanglement distribution protocols: a) classical entanglement percolation on the original lattice and b) QEP consisting of creating two decoupled lattices (the square and triangular lattices) via entanglement swapping, followed by CEP on each of the resulting lattices. The transformation is described in Fig. 12. Note that, for $p' = 0$, the initial lattice is a triangular lattice with serial double bonds and therefore the critical point $p = \sqrt{p_c(\Delta)} \approx 0.589$. On the other hand for $p = 0$ and $p' \neq 0$ the initial lattice is the kagomé lattice.

We first examine the most robust measure of a protocol's effectiveness—the binary measure that tells whether long-range entanglement is possible or not. The phase diagrams for this example before and after the transformation are shown in Fig. 13. We see that there are regions in the phase space for which QEP is better than CEP, and vice versa.

In the region in which both protocols allow long-range entanglement, a more detailed measure similar to those in previous sections is necessary. For example, for $p = p'$, we performed an analysis similar to the one used for doubling the square lattice. The two critical boundaries intersect at $p = p' = p_c(\Delta)$, but comparing connectivity just above the critical point shows that the transformation does not improve the probability of long-range entanglement. Likewise for $p = p'$ and p near 1, series expansions showed that the transformation is not an improvement on CEP. We have not yet determined whether

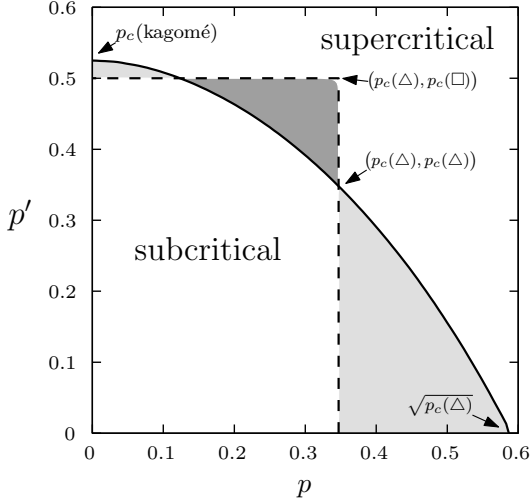


FIG. 13: Phase diagram for the asymmetric triangular lattice. The heavy solid curve (obtained by Monte Carlo) separates the supercritical and subcritical regions on the original asymmetric triangular lattice (CEP). The dashed curve composed of two line segments separates the supercritical and subcritical regions after the transformation (QEP). After transformation, the supercritical region is defined to be the region for which at least one of the disjoint lattices is supercritical. In the light gray regions, long-range entanglement is possible with QEP, but not with CEP. In the dark gray region it is possible with CEP, but not with QEP.

QEP in this scenario succeeds for some other $p = p'$, but this seems unlikely.

IV. CONCLUSIONS

In this paper we have considered the problem of establishing long-distance entanglement in quantum pure-state networks on regular 2D lattices. We have discussed in detail several examples of quantum entanglement percolation strategies that are better than the corresponding classical strategies, i.e. those consisting of a direct attempt to convert bonds into singlets. Our results illustrate nicely the interplay between quantum information theory and classical percolation theory. Despite the fact that we do find certain rules and regularities governing QEP strategies, many questions remain open. For instance, we cannot say anything about optimality of our QEP protocols—and most probably they are not optimal. All of our protocols involve LOCC acting on pairs of qubits only; can multipartite LOCC, which leads inevitably to creation of multipartite entanglement, help? We know that for sufficiently large initial entanglement, perfect entanglement between remote nodes may be established with distance-independent probability $P > 0$. Is it also possible for arbitrarily small initial entanglement?

Acknowledgements

We thank A. Acín, J.I. Cirac, and D. Cavalcanti for discussions. We thank S. Perseguers for kindly supplying figures. We acknowledge support of the EU IP Programme “SCALA”, and Spanish MEC grants (FIS 2005-04627, Consolider Ingenio 2010 “QOIT”). J.W. thanks Lluís Torner and ICFO for hospitality. He was partially supported by NSF grant DMS 0623941. M. L. thanks also the Alexander von Humboldt Foundation for support.

APPENDIX A: MAJORIZATION THEORY

Majorization theory has been applied to questions of transforming one bipartite pure state to another by LOCC. In particular, a theorem due to Vidal[18] gives the probability that such a transformation can be achieved via an optimal protocol (without specifying that protocol.) We state the result and apply it to the distillation procedure used in this paper. We must first introduce a certain partial order on vectors. Consider two real, d -dimensional vectors \mathbf{r} and \mathbf{s} . We define the vector \mathbf{r}^\uparrow by reordering the elements of \mathbf{r} into non-decreasing order, and likewise with \mathbf{s} . We say that \mathbf{r} is submajorized by \mathbf{s} , denoted by $\mathbf{r} \prec^w \mathbf{s}$, if

$$\sum_{i=0}^k r_i^\uparrow \geq \sum_{i=0}^k s_i^\uparrow, \quad (\text{A1})$$

for all $k = 0, \dots, d-1$. Denoting the vector of Schmidt coefficients of ψ by $\boldsymbol{\lambda}(\psi)$, the theorem states that $|\psi\rangle$ can be transformed into $|\phi\rangle$ with probability p , where p is the largest number on $[0, 1]$ such that $\boldsymbol{\lambda}(\psi) \prec^w p\boldsymbol{\lambda}(\phi)$.

A simple, relevant application is the computation of the probability that optimal conversion of a state $|\psi\rangle \in \mathbb{C}^d \otimes \mathbb{C}^d$ to a singlet will succeed. Application of (A1) gives $p = \min\{1, 2(1 - \alpha_0)\}$.

Now we consider distillation, defined here as the optimal protocol for converting n pure states $|\alpha_i\rangle \in \mathbb{C}^2 \otimes \mathbb{C}^2$ to $n-1$ product states and one maximally entangled state in the Schmidt bases. This operation is useful, for instance, in attempting to get a single, maximally-entangled bond from n bonds connecting two nodes. Explicitly,

$$|\alpha_i\rangle = \sqrt{\alpha_{i,0}}|00\rangle_i + \sqrt{\alpha_{i,1}}|11\rangle_i,$$

with $\alpha_{i,0} \geq \alpha_{i,1}$ and elements of the ordered set $(\alpha_{0,0}, \alpha_{1,0}, \dots, \alpha_{n-1,0})$ non-increasing. As usual, $|jk\rangle_i$ is shorthand for $|j\rangle_{i,0} \otimes |k\rangle_{i,1}$. For $\mathbf{j} \in \{0,1\}^n$ define the bijective numeration $k(\mathbf{j}) = \sum_{i=0}^{n-1} 10^i j_i$ and $\gamma_k = \gamma_k(\boldsymbol{\alpha}) = \alpha_{0,j_0} \alpha_{1,j_1} \cdots \alpha_{n-1,j_{n-1}}$. Then we can write

$$\bigotimes_{i=0}^{n-1} |\alpha_i\rangle = \sum_{\mathbf{j}: k(\mathbf{j})=0}^{2^n-1} \sqrt{\gamma_k} \bigotimes_{m=0}^{n-1} |j_m j_m\rangle_m. \quad (\text{A2})$$

In order to apply the theorem, we need to show that this state can be written as a bipartite state with Schmidt coefficients that can be chosen to satisfy our distillation condition. To this end collect all the first qubits of the bipartite states and all the second qubits, defining

$$|k(\mathbf{j})\rangle_a = \bigotimes_{i=0}^{n-1} |j_i\rangle_{i,0} \quad \text{and} \quad |k(\mathbf{j})\rangle_b = \bigotimes_{i=0}^{n-1} |j_i\rangle_{i,1},$$

so that (A2) becomes

$$\bigotimes_{i=0}^{n-1} |\alpha_i\rangle = \sum_{\mathbf{j}: k(\mathbf{j})=0}^{2^n-1} \sqrt{\gamma_k} |k(\mathbf{j})\rangle_a |k(\mathbf{j})\rangle_b. \quad (\text{A3})$$

Note that $\sum_{k=0}^{2^n-1} \gamma_k = \prod_{i=0}^{n-1} (\alpha_{i,0} + \alpha_{i,1}) = 1^n = 1$ so that (A3) defines a state in $\mathbb{C}^{2^n} \otimes \mathbb{C}^{2^n}$ already in Schmidt form. The submajorization condition is

$$(\gamma_{2^n-1}, \gamma_{2^n-2}, \dots, \gamma_0) \prec^w \left(0, 0, \dots, \frac{p}{2}, \frac{p}{2}\right),$$

for which the only nontrivial inequality is the penultimate one $1 - \gamma_0 \geq p/2$. Thus the maximum distillation probability is

$$p = \min \{1, 2(1 - \alpha_{0,0}\alpha_{1,0} \cdots \alpha_{n-1,0})\}.$$

Note that this result agrees with the special case in (3).

APPENDIX B: MONTE CARLO ESTIMATES OF $\theta(p)$ AND $\pi(p)$

We computed Monte Carlo estimates of $\theta(p)$ and $\pi(p)$ using the Hoshen-Kopelman [22] algorithm with modifications for efficiency [23] and the Mersenne twister [24] random number generator. Together with series expansions and exactly known critical densities, the quality of the data we obtained is more than sufficient to determine which transformations are advantageous. We estimated $\theta(p)$ by computing the mean density of the largest cluster on an $L \times L$ lattice. Near the critical density we typically used lattices of size $L = 2-5 \times 10^5$. We took the value of L at the inflection point of plots of $\theta(p)$ *v.s.* L at fixed p as estimates of the correlation length $\xi(p)$. We typically found that $\xi(p) > L$ for $p - p_c < 0.0005$. We only expect significant systematic error in this region, but this poses no problem because the curves are never close to one another in these regions. (We reformulated the problem when this is the case.) We computed statistical error, but the error bars are at most barely visible on the plots, so we omitted them. Exceptions are very near $p = p_c$ where fluctuations in the size of the largest cluster become large, and near $p = 1$, where finite clusters are rare, so collecting sufficient samples to distinguish curves is too expensive. We discuss the effects of these errors in the main body of the paper.

We wrote a single computer code to study all the lattices. The code supports lattices with vertices that occupy points on \mathbb{Z}^2 with bonds connecting each pair of nearest neighbors as well as a diagonal bond from (i, j) to $(i+1, j+1)$. Because the connectivity properties that we calculated depend only on the graph structure of the lattice, we embedded the graph of each lattice in the square lattice plus diagonals described above. Depending on the lattice being modeled, some of the bonds in the underlying lattice are closed with probability one, and some are open with probability one, with the vertices identified in the embedded lattice. The graph structures of all lattices appearing in this paper were modeled in this way.

APPENDIX C: SERIES EXPANSIONS

We follow the ideas of the perimeter method [25, 26, 27] to compute high-density series expansions of $\theta(p)$ and $\pi(p)$ listed in Table II. Here we discuss the method for computing the series for $\theta(p)$, but our method for computing $\pi(p)$ is similar. Here, a cluster is any connected subgraph that contains at least one vertex. We denote by \mathcal{S}_0 the collection of all finite clusters that include the vertex at the origin, and by \mathcal{S} the partition of \mathcal{S}_0 induced by equivalence under translation, in other words the collection of free clusters. Choosing an enumeration α_j of clusters in \mathcal{S} , the probability that a randomly selected site is in the infinite open cluster is easily seen to be

$$\theta(p) = 1 - \sum_{j=1}^{\infty} s_j (1-q)^{b_j} q^{t_j},$$

where s_j is the number of sites and b_j the number of bonds in cluster α_j , and t_j is the number of perimeter bonds (bonds adjacent to cluster α_j). Clearly, we can find the series expansion in q by enumerating the clusters in an order that is non-decreasing in t_j . For instance, on the hexagonal lattice, only the cluster consisting of an isolated site has a perimeter t of size less than or equal to 3 (see Fig. 14), so that to lowest non-trivial order $\theta(p) = 1 - q^3$. Percolation theory is a difficult subject precisely because the full enumeration is difficult. The series for θ_{Δ} (for bond percolation) was calculated by machine to high order in Ref. 27. Although tables of cluster numbers have been published, all the others that we are aware of are either for site percolation or for bond percolation with cluster size measured by the number of bonds rather than sites (neither of which can be mapped to our problem.)

For our results we counted a few small clusters by hand, which is not so difficult. In practice however, we find that it is also essential to categorize the clusters by symmetry. As an example, the clusters contributing to θ on the hexagonal lattice to sixth order in q are shown in Fig. 14.

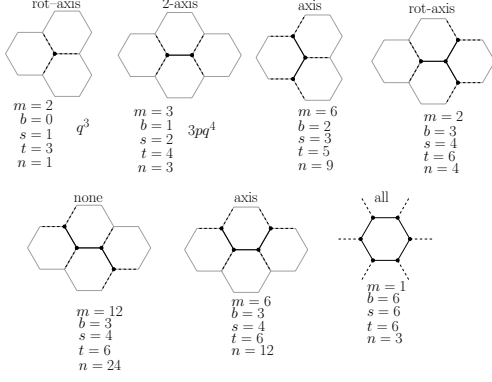


FIG. 14: Clusters on the hexagonal lattice contributing to θ to sixth order in q . Symmetries and multiplicities m are: none–12, one axis–6, rotation–4, two axes–3, rotation and axis–2, all–1. The number of contributing clusters per figure is given by $n = ms/2$, the factor of 1/2 accounting for the fact that each site only supports half the rotations. The contribution to θ is then $-ms(1 - q)^b q^t/2$.

-
- [1] R. Horodecki, P. Horodecki, M. Horodecki, and K. Horodecki, Rev. Mod. Phys. , in press, arXiv:quant-ph/0702225v2.
- [2] J. I. Cirac, P. Zoller, H. J. Kimble, and H. Mabuchi, Phys. Rev. Lett. **78**, 3221 (1997), arXiv:quant-ph/9611017v1.
- [3] A. D. Boozer, A. Boca, R. Miller, T. E. Northup, and H. J. Kimble, Phys. Rev. Lett. **98**, 193601 (pages 4) (2007), arXiv:quant-ph/0702248v1, URL <http://link.aps.org/abstract/PRL/v98/e193601>.
- [4] A. K. Ekert, Phys. Rev. Lett. **67**, 661 (1991).
- [5] C. H. Bennett, G. Brassard, C. Crépeau, R. Jozsa, A. Peres, and W. K. Wootters, Phys. Rev. Lett. **70**, 1895 (1993).
- [6] A. Poppe, M. Peev, O. Maurhart, and (on behalf of the Integrated European Project SECOQC), Int. J. Quant. Inf. **6**, 209 (2008), arXiv:quant-ph/0701168.
- [7] J. I. Cirac, A. K. Ekert, S. F. Huelga, and C. Macchiavello, Phys. Rev. A **59**, 4249 (1999), arXiv:quant-ph/9803017v2.
- [8] M. Nielsen and I. Chuang, *Quantum Computation and Quantum Information* (Cambridge University Press, Cambridge, 2000).
- [9] H.-J. Briegel, W. Dür, J. I. Cirac, and P. Zoller, Phys. Rev. Lett. **81**, 5932 (1998), arXiv:quant-ph/9803056v1.
- [10] W. Dür, H.-J. Briegel, J. I. Cirac, and P. Zoller, Phys. Rev. A **59**, 169 (1999), arXiv:quant-ph/9808065v1.
- [11] L. Childress, J. M. Taylor, A. S. Sorensen, and M. D. Lukin, Phys. Rev. A **72**, 052330 (pages 16) (2005), arXiv:quant-ph/0502112, URL <http://link.aps.org/abstract/PRA/v72/e052330>.
- [12] L. Hartmann, B. Kraus, H.-J. Briegel, and W. Dur, Phys. Rev. A **75**, 032310 (pages 17) (2007), arXiv:quant-ph/0610113, URL <http://link.aps.org/abstract/PRA/v75/e032310>.
- [13] M. Żukowski, A. Zeilinger, M. A. Horne, and A. K. Ekert, Phys. Rev. Lett. **71**, 4287 (1993).
- [14] A. Acín, J. I. Cirac, and M. Lewenstein, Nature Physics **3**, 256 (2007), arXiv:quant-ph/0612167, URL <http://dx.doi.org/10.1038/nphys549>.
- [15] S. Perseguers, J. I. Cirac, A. Acín, M. Lewenstein, and J. Wehr, Phys. Rev. A **77**, 022308 (pages 14) (2008), arXiv:0708.1025, URL <http://link.aps.org/abstract/PRA/v77/e022308>.
- [16] K. Kieliing and J. Eisert, in *Quantum Percolation and Breakdown* (Springer, Heidelberg, 2008), in press, arXiv:0712.1836.
- [17] G. Vidal, Phys. Rev. Lett. **83**, 1046 (1999), arXiv:quant-ph/9902033.
- [18] M. A. Nielsen and G. Vidal, Quantum Inf. Comput. **1**, 76 (2001).
- [19] G. Grimmett, *Percolation* (Springer-Verlag, Berlin, 1999), 2nd ed.
- [20] D. Stauffer and A. Aharony, *Introduction to Percolation Theory* (Taylor & Francis, London, 1992), 2nd ed.
- [21] R. M. Ziff and P. N. Suding, J. Phys. A **30**, 5351 (1997), arXiv:cond-mat/9707110.
- [22] J. Hoshen and R. Kopelman, Phys. Rev. B **14**, 3438 (1976).
- [23] H. Nakanishi and H. E. Stanley, Phys. Rev. B **22**, 2466 (1980).
- [24] T. Nishimura, ACM Trans. on Modeling and Computer Simulation **10**, 348 (2000).
- [25] C. Domb, Nature **184**, 589 (1959).
- [26] C. Domb and M. F. Sykes, Phys. Rev. **122**, 77 (1961).
- [27] J. Blease, J. W. Essam, and C. M. Place, J. Phys. C. **11**, 4009 (1978).